Energy Conversion and Management: X 22 (2024) 100596

Contents lists available at ScienceDirect

Energy Conversion and Management: X

journal homepage: www.sciencedirect.com/journal/energy-conversion-and-management-x

Energy analysis and numerical evaluation of the decanter centrifuge for wastewater management to allow a sustainable energy planning of the process

Alessandro Leone [a], Claudio Perone [b,*], Antonio Berardi [a], Antonia Tamborrino [a]

[a] Department of Soil, Plant and Food Science (DISSPA), University of Bari Aldo Moro, Via Amendola 165/a, 70126 Bari, Italy
[b] Department of Agriculture, Food, Natural Resource and Engineering, University of Foggia, 71122 Foggia, Italy

ARTICLE INFO

Keywords:
Energy model
Decanter centrifuge
Sludge dewatering
Regenerative VFD
Energy efficiency

ABSTRACT

The decanter-centrifuge is widely used for dewatering and thickening of civil and industrial sludge. The latest generation decanters, both the bowl motors (main) and the screw (back-drive) are often driven by variable-frequency drives (VFD), with the back-drive able to recover the energy during braking. We created a decanter centrifuge energy model equipped with a braking recovery system during the sludge dewatering process, with the aim of identifying its optimal operating conditions for both energy consumption and product quality. Specific models at 15–20–25 $m^3\ h^{-1}$ and various differentials speed (Δn) were used to derive a general model, then validated with experiments at 18–20 $m^3\ h^{-1}$. Specific models used to identify the best operating conditions in terms of specific energy (e) and energy recovery (E_{Rec}) show that at 15–20–25 $m^3\ h^{-1}$ the lowest energy consumptions were 1.88–1.76–1.57 kWh m^{-3}, respectively, instead, E_{Rec} was 5.88–0.31–12.10 kW respectively, highlighting that a high recovery is not necessarily linked to an increased energy saving. The accuracy of these models was confirmed by high values of correlation coefficients R^2 and very low Root Mean Square Errors (RMSE) in each case. The general model, extrapolated from the specific models, makes it possible to predict specific consumptions at different flow rates within the operating range of the decanter. This was validated with an experimental test at 18–20 $m^3\ h^{-1}$ with R^2 above 97 % and RMSE 2,59E-02 kWh m^3. The dry matter content in the cake decreases when the Δn or the feed rate increases.

In conclusion, the decanter centrifuge model could represent a useful tool for optimizing the sludge dehydration process.

1. Introduction

Electricity consumption in the world has been steadily increasing over the past few decades as more countries become industrialized and the population continues to grow [1–3]. According to the International Energy Agency (IEA) the industrial sector is a major consumer of electricity, accounting for approximately 37 % of global energy consumption in 2019.

While electricity has brought many benefits to modern society, it also has significant environmental impacts that must be addressed to ensure long-term sustainability [4].

One of the biggest environmental impacts of electricity consumption is greenhouse gas emissions. In fact, the generation of electricity is a major source of these, primarily from the burning of fossil fuels such as coal, oil, and natural gas [5–7]. Emissions are the main cause of global warming and consequent climate change. The consequences of climate change are severe and wide-ranging, including severe weather events, droughts, rising sea levels, floods, more frequent and severe natural disasters, loss of biodiversity, and negative impacts on human health and well-being [8–10].

Electric energy saving is an important aspect of sustainability, as it can help to reduce the environmental impact of human activities and preserve natural resources for future generations.

Manufacturing industries generate significant environmental impacts owing to a considerable energy consumption: about 25 % of total worldwide industrial energy consumption is attributed to machining processes only [11].

A considerable part of the electric energy in the industrial sector is

* Corresponding author.
E-mail address: claudio.perone@unifg.it (C. Perone).

https://doi.org/10.1016/j.ecmx.2024.100596
Received 22 March 2024; Received in revised form 15 April 2024; Accepted 16 April 2024
Available online 18 April 2024
2590-1745/© 2024 The Author(s). Published by Elsevier Ltd. This is an open access article under the CC BY-NC-ND license (http://creativecommons.org/licenses/by-nc-nd/4.0/).

used by electric motors to drive machines. In this case, reducing energy consumption can include different strategies such as:

- Optimize the mechanical design of the machines to make them more efficient [12]
- Optimize motor sizing, by choosing the right size for an application can help reduce energy [13].
- Improve ordinary and extraordinary maintenance programs: in fact regular maintenance can ensure that motors are running at their optimal level and reduce energy losses [14,15].
- Utilization of high-efficiency motors [16,17].
- Implementation of variable-frequency drive (VFD) as a motor controller to optimize the use of energy [18].

In addition, for machines driven by an electric motor, establishing a model of energy consumption according to the different machine operating conditions is the basis to reduce energy consumption. The lack of a real and accurate energy consumption model hinders the implementation of effective strategies such as planning and scheduling efficient processes for energy consumption and performance [19–21].

Energy modelling of machines involves creating a mathematical or computer-based model of the machine's energy consumption and performance characteristics [22]. The purpose of energy modelling is to optimize the design and operation of the machine to minimize energy consumption while maintaining or improving performance [23–25].

Energy modelling can be used for a wide range of machines [26,27]. By way of explanation but not exhaustively, energy modelling has been carried out to optimize the energy performance in food industry [28–31], in machining operation [32,33,21] and also in sludge dewatering [34–16].

One of the innumerable machines used both in the industry and food processing, and which often has a central role in a plant, even from an energy consumption point of view, is the decanter centrifuge (Alan Records, Decanters 2001).

The Decanter Centrifuge is used to separate solid particles from liquids in a continuous manner, by using centrifugal forces that can be well over 3000 times greater than gravity [35]. The decanter is used widely in food processing, especially in liquid food separation, like olive oil, juice, palm oil, beverage, casein fractionation etc. [36–40].

The decanter is also widely used in all purification plants for the dewatering of civil and industrial sludge [41]. The aim of dewatering is to increase the solids concentration and to decrease the free water, with the aim to facilitate its transportation and to minimize the load on the downstream processes, such as composting, anaerobic digestion or simply to reduce the volumes to be disposed of or the transfer to incinerators [42].

The core of the decanter is made up of a horizontal bowl with a cylindrical and conical shape with a coaxial screw on its inside. The bowl and screw rotate at a differential speed (Δn). During the process the sludge is pumped into the bowl through the hollow axis of the screw, the centrifugal force causes the solid liquid separation according to their density. While the screw transfers the solids to the conical end of the bowl forcing them through discharge nozzles, the fluids escape towards the outlet placed at the cylindrical end of the bowl [43–45].

The Δn regulates the discharge flow rate of solids from the bowl, while allowing the sludge feed rate to be adjusted. Furthermore, the drying of the solids can be chosen by varying the Δn and consequently the residence time of the sludge in the bowl [46].

In the latest generation decanters, the bowl is driven by a main motor and the screw bis driven by a second motor called a back-drive. Both motors are controlled by variable-frequency drives (VFD) with regenerative braking systems. In a regenerative braking system the electric power delivered to the motor is regenerated while the motor decelerates by applying negative torque to the motor shaft, and since energy storage capacity inside the VFD is very limited, regenerative energy could be returned to the grid or quickly dissipated by a braking resistor [47]. When a wound rotor induction motor (WRIM) is used, the sliprings allow easy recovery of the slip power that can be electronically controlled to vary the speed of the induction motor. [48]. Instead of dissipating this power in external resistors, it can be regenerated in a slip power recovery system (SPRS), such as a regenerative converter [49].

When a decanter works in back-drive configuration, the electric motor of the screw can take the mechanical torque during the process and turn it into electrical energy to return to the main grid or to share with the main motor through a DC bus connection between the VFDs [28]. During the process the energy regenerated depends on the characteristics of the incoming wastewater (% dry matter) and on the combination of the machine operating parameters such as load conditions of the centrifuge (flow rate) and differential speed (Δn).

However, since the mapping of energy consumption is not known, the process planner, although in the presence of machines with energy saving systems, only adjusts the machine according to the final performance and not according to the relationship between performance and energy consumption. The lack of energy mapping does not allow an efficient energy saving.

In the present study, we carried out an energy consumption modelling of a centrifugal decanter implemented with an energy recovery system during the sludge dewatering process.

The purpose of the study is to identify the optimal operating conditions of the decanter to minimize its energy consumption while maintaining performance, thus providing the process planners with a useful tool to guide their decisions.

2. Materials and methods

2.1. Industrial plant for wastewater treatment

The experimental plan developed was carried out at an industrial plant for the treatment of domestic and industrial wastewater that included the following processing stages:

- coarse and fine screening
- grease removal
- clariflocculation
- flow equalization
- primary sedimentation
- aerobic stabilization
- secondary sedimentation
- centrifugal dewatering.

The present research focuses on the centrifugal dewatering, the process of which is shown in the Fig. 1.

After the secondary sedimentation, the outgoing wastewater with dry matter in the range 1–3 % was added to a previously water diluted liquid polymer and then pumped to the horizontal two-phase centrifuge. At the exit of the centrifuge, clarified water and dehydrated solid sludge with a dry substance content generally higher than 20 % were collected separately.

Depending on the company management model, the outgoing sludge can be disposed of in a field, sent to a composting process or disposed of in landfills.

2.2. Decanter centrifuge with regenerative system

The phase of the wastewater treatment process involved in the present study was the centrifugal dewatering of the sludge coming from the aerobic stabilization with the use of a regenerative back-drive decanter with double electric motor. The rotation of the bowl is driven by a 75 kW main motor (M1), while the rotation of the scroll is driven by a 30 kW back-drive motor (M2).

Both motor M1 and motor M2 are equipped with variable-frequency drive device VFD1 and VFD2. The VFD2 inverter is of the regenerative

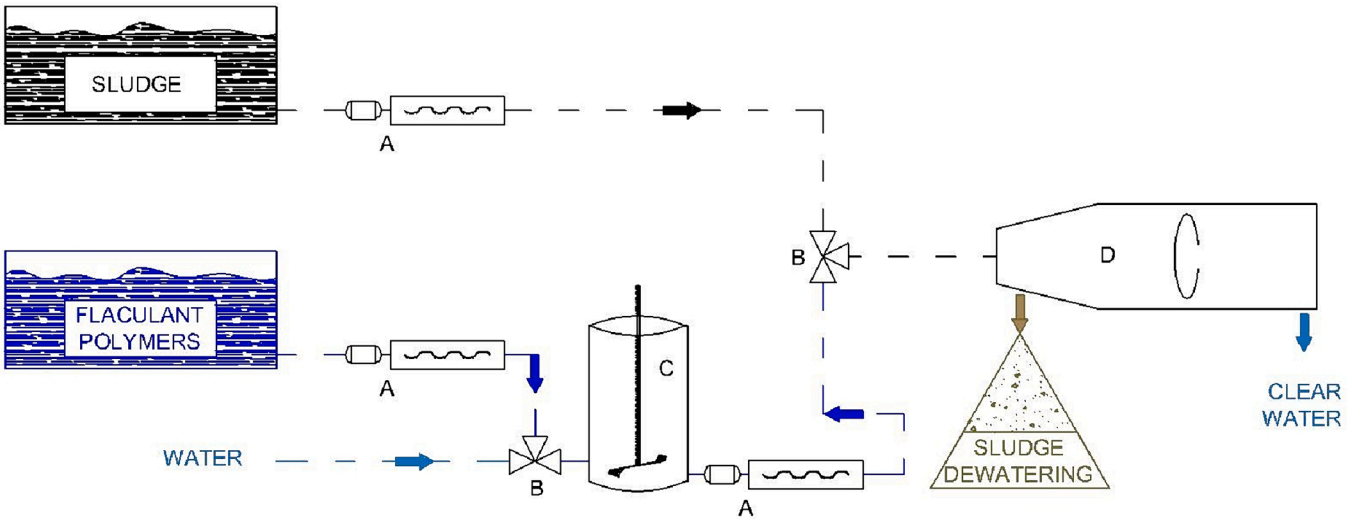

Fig. 1. Centrifugal dewatering process.

type. The VFD2 inverter allows energy to be recovered and fed into the grid, so that it can be used to power other equipment. The VFD contains all the components needed to operate in regenerative mode, from the active power supply to the LCL line filter. The active power supply maintains full power flow in both motor and generation modes. Therefore, the back-drive motor M2, working in regenerative mode, recovers energy through the DC-BUS to feed the main motor M1 (Fig. 2).

During the centrifugal dewatering, the rotor of the back-drive motor spins faster than the winding frequency, sustaining a magnetic field that generates power back into the line. In fact, the back-drive motor rotates the scroll at a lower speed compared to the bowl, through a gear box, but because of the torques and friction created in rotating the sludge (liquid and solids) filling the bowl, the conveyor will want to rotate at the speed of the bowl [50]. As a consequence, the back-drive motor usually acts as a brake, receiving energy and thus in regenerative mode.

During regeneration, the regenerative energy available in the inverter front end of VFD2, is used to supply M1 through a regenerative converter circuit parallel to the drive inverter circuit and the DC bus. The two VFDs are connected in a circuit, via the DC bus stage. The common DC bus allows the two separate VFDs to share power. So, when the regenerative VFD is in regeneration mode, the motoring VFD can pull power from the DC bus in addition to the grid. In this way, the regeneration power is shared between the VFDs controlling M1 and M2 motors and not sent back to the mains.

When also M2 is in motoring mode, the regenerative VFDs transfer power from the mains to the motor terminals, without loss in the regenerative converter. Regenerative drives replace the input rectifiers with insulated-gate bipolar transistors (IGBTs). These IGBTs act as the input rectifiers but provide the opportunity for bi-directional power flow. The regenerative converter will be activated because the regenerative energy charges the DC link capacitors of the variable frequency drives [47]. Ultimately, when the motor generates power, it flows into the regenerative drive and then to M1 by reducing the overall energy consumption of the application and hence lowers total energy costs.

However, to keep the load balanced, each drive rectifier channel must share a balance of the load. This load sharing would result in about 66 % of the load carried by the main drive and 33 % of the load carried by the regenerative drive [51].

2.1. *Electrical measurement system*

In order to measure the energy consumption during the operation of the decanter under the different test conditions, an energy measurement chain was implemented on the electrical panel of the decanter. In detail,

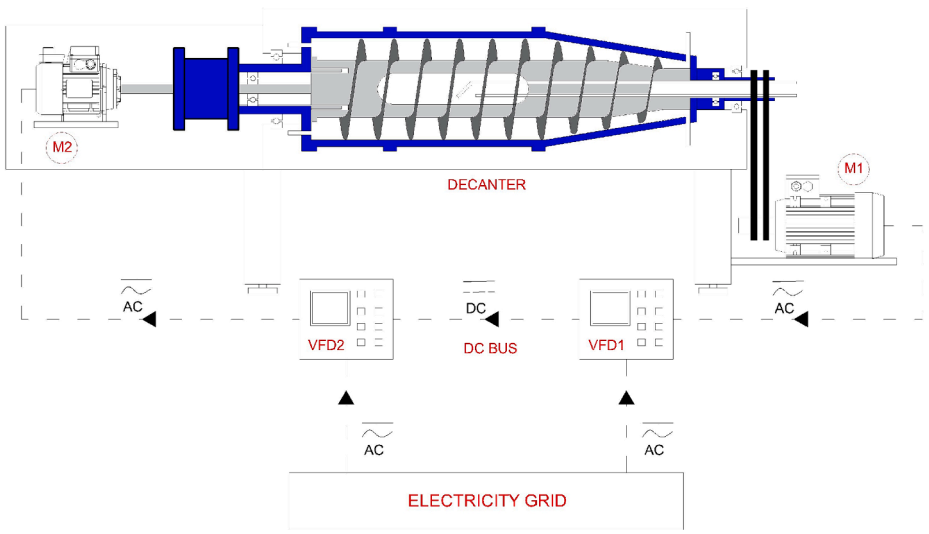

Fig. 2. Decanter with backdrive control.

4 energy meters (EM001, EM002, EM003and EM004) were installed as shown in Fig. 3.

Three energy meters EM001 and EM003 (Lovato DMG 210, Milano, Italy) and EM003 (Lovato DMG 300, Milano, Italy) were installed to measure the AC in three different points of the electrical system. EM001 and EM002 detected the electrical energy absorption from the mains upstream of the main motor and back drive VFDs, respectively. Similarly, EM003 measured the energy absorbed by the main motor M1. In fact, as indicated by the double direction arrow on the line between VFD2 and back-drive in Fig. 3, M2 could work in both active or regenerative mode. The energy balance reported in Eq. (1) allowed to deduce the amount of energy recovered or absorbed by the back drive (E_{Rec}):

$$E_{Rec} = E_{EM003} - (E_{EM001} + E_{EM002}) \begin{cases} if\, E_{Rec} > 0 regenerative mode \\ if\, E_{Rec} < 0 active mode \end{cases} \quad (1)$$

A portable energy meter EM004 (Fluke model 1732) was used on the DC bus connection between the two inverters to measure and validate the E_{Rec} values through sample measurements made during all tests of the regenerative power. TEmeter® software was used to manage the measurement chain. TEmeter® is a software system that allows you to acquire data through embedded servers, installed in the field, which send these to a cloud storage system making them available through a web portal on the internet with restricted access. The system acquires the data sampled from the instrumentation, with a frequency depending on the characteristics of the measuring device and makes them available on the web portal in roughly 6 s from their reading. The historical data is aggregated every 15 min and stored. The real-time data is available on the site through a user-friendly dashboard, updated every 30 s, including the historical data. The communication between the embedded servers and the cloud system is fully encrypted with SSL, as is access to the web portal.

During the tests, the TEmeter® system was connected to compact network analysers for use in three-phase three-wire systems with unbalanced load, to allow real-time display and subsequent archiving of the main quantities of an electric network and in particular:

- Equivalent phase voltages and currents;
- Equivalent active and reactive power;
- Total displacement factor (cosφ);
- Frequency;
- Bidirectional active and reactive energy.

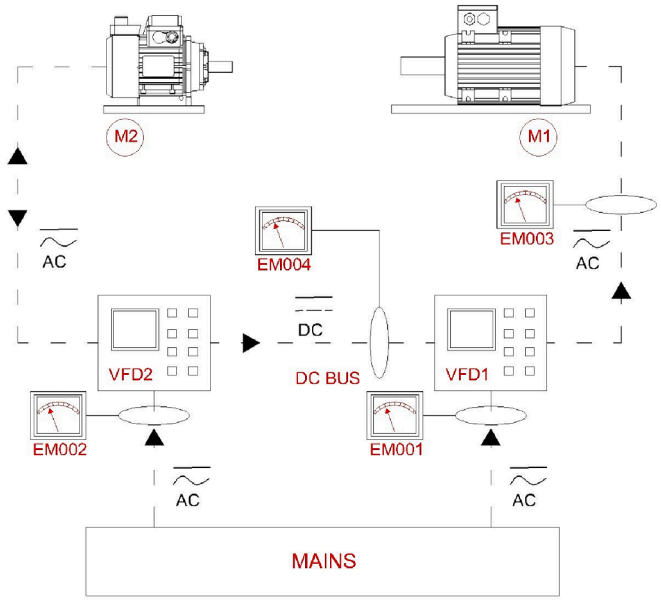

Fig. 3. Wiring diagram implemented with energy measurement chain.

2.2. Energy consumption modelling procedure

To obtain the modelling of the energy consumption of the decanter, experimental tests were carried out on sludge dewatering under different decanter operating modes.

The decanter was fed with five different flow rates (in the minimum–maximum range allowed by the machine specifications) and at different variations of rpm between bowl and screw (Δn). In all tests the rotation speed of the bowl was 2600 rpm.

Table 1 shows the plan of experimental tests.

Specific models for three flow rate value (15 $m^3\ h^{-1}$, 20 $m^3\ h^{-1}$ and 25 $m^3\ h^{-1}$) and a general model of all feed flow values were trained and tested.

For the specific model for each sludge flow rate, six Δn values within the specific operating range of the decanter were selected of which four were used to train the model and two to test the model.

For the general model the data of the best energy performances at 15 $m^3\ h^{-1}$, 20 $m^3\ h^{-1}$ and 25 $m^3\ h^{-1}$ were used to train the model, while two further measurements at a flow rate of 18 $m^3\ h^{-1}$ and 22 $m^3\ h^{-1}$ with three Δn values each, were used to test it. For both the specific and general models, a quadratic polynomial was used, which is the one that best fits all the experimental data.

The Δn values were chosen by carrying out preliminary sludge dehydration tests. Specifically, during the preliminary tests for each chosen flow rate value, the minimum value of Δn identified was the one below which the decanter went into protection mode due to excessive torque resistance on the screw, while the highest value was the one above which the decanter went into protection mode due to the sludge exiting from the clear liquid weir. Once the minimum and maximum limits of Δn were identified, the other intermediate values were chosen.

Each single measurement test lasted 60 min. Whenever the test conditions changed, the first 15 min of processing were not considered, as they were necessary for the stabilization of the decanter. Each

Table 1
Experimental plan divided into training and testing trials for both specific and general models.

Δn [rpm]	Sludge flow rate [$m^3\ h^{-1}$]	Specific flow rate model [Training/testing]	General model [Training/testing]
3.0	15	Training	Training
3.2		Training	
3.5		Testing	
4,0		Training	
4,2		Testing	
4.5		Training	
3	18	–	Testing
4		–	
5		–	
3	20	Training	Training
3.5		Testing	
4		Training	
4.5		Testing	
5		Training	
6		Training	
4	22	–	Testing
5		–	
6		–	
4.3	25	Training	Training
4.4		Testing	
4.5		Training	
4.6		Training	
4.8		Testing	
4.9		Training	

individual test condition was repeated three times.

From the TEmeter® system, for the entire monitoring period, the main quantities of an electric network were detected with frequency per minute as averages of the previous 60 s.

In all the tests carried out, 2.5 % of liquid polymer was added to the inlet sludge.

2.3. Sampling and laboratory analyses

During the energy consumption monitoring, the incoming sludge and the solid and liquid phases exiting the decanter were sampled. For all samples taken the moisture content was determined according to UNI EN 12880:2002.

2.4. Statistical analyses

The energy consumption results were evaluated statistically with One-way ANOVA with post-hoc Tukey HSD test, while the dryness of the waste and cake data were evaluated statistically with Kruskal Wallis and post-hoc Dunn's test.

The validation of the proposed model is investigated by using Root Mean Square Error (RMSE) and correlation coefficient (R^2).

The root-mean-square error (RMSE) expressed as:

$$RMSE = \sqrt{\frac{\sum_{i=1}^{N}\left(P_{pred,i} - P_{meas,i}\right)^2}{N}} \tag{2}$$

and the correlation coefficient is calculated using the following equation:

$$R^2 = \left(\frac{\sum_{i=1}^{N}(P_{meas,i} - P_{meas,avg})(P_{pred,i} - P_{pred,avg})}{\sqrt{\sum_{i=1}^{N}(P_{meas,i} - P_{meas,avg}) \sum_{i=1}^{N}(P_{pred,i} - P_{pred,avg})}} \right)^2 \tag{3}$$

where P_{pred} and P_{meas} are respectively predicted and measured values.

3. Results and discussion

The data processing of the energy measurements aimed to model the energy consumption for each flow rate. Subsequently, the specific models obtained were used to produce the general model to predict the behaviour of the decanter at different sludge flow rates.

3.1. Energy consumptions at specific flow rates

In Tables 2, 3 and 4 the energy performance results for each flow rate at different Δn are shown. The tables report the mean values (μ) and standard deviations (σ) of instantaneous power drawn from the mains by VFD1 (E_{EM001}) and VFD2 (E_{EM002}), and the power required by the main motor (E_{EM003}). Equation (1) returns the energy recovered from the back-drive (E_{Rec}), while the sum of the measurements of EM001 and EM002, which represent the power absorbed from the grid, allowed to evaluate the specific energy (e) for each sludge flow rare ($\dot{V}_s$):

$$e = \frac{(E_{EM001} + E_{EM002})}{\dot{V}_s} \tag{4}$$

At $\dot{V}_s$ equal to 15 $m^3\ h^{-1}$, the energy demand of the main motor M1 decreased by about 18.7 % from the Δn 3 to the Δn 4.5. However, the energy recovered from the back-drive reduced significantly by about 59.4 %. As a result, the specific energy underwent a slight reduction of about 3.67 %. A4 to A6 test settings represent the best conditions at 15 $m^3\ h^{-1}$ in terms of energy savings (1.88 kWh m^{-3}).

At $\dot{V}_s$ equal to 20 $m^3\ h^{-1}$ the energy absorbed by the main motor M1 decreased by about 35.9 % passing from Δn 3.0 to 6.0, while the back-drive stopped recovering and started working actively, albeit with a small power demand. Since the power reduction requested by M1 was greater than the recovered power reduction, in absolute terms, the specific energy consumed in any case showed a reduction of about 9.1 %. The best conditions in terms of energy savings were reached under C5 configuration (1.76 kWh m^{-3}), where, although energy recovery was essentially nil, the lowest specific consumption for sludge processing was observed. Even at Δn 6.0 the specific energy was substantially the same (1.77 kWh m^{-3}), since the total power request by the main motor was lower by about the same quantity required by the back drive, probably due to torque compensation.

At 25 $m^3\ h^{-1}$ of sludge flow rate, the energy absorbed by the main motor showed a slight decrease, only about 3.6 % passing from Δn 4.3 to 4.9, while the back-drive recovery remained almost the same up to Δn 4.6 and then decreased by about 21.2 %. In this configuration the power reduction requested by M1 is lesser than the recovered one, and thus the specific energy increase was about 1.7 % (1.65 kWh m^{-3}). In this restricted range of operation of the Δn, the greater energy saving is reached at Δn equal to 4.6 (1.57 kWh m^{-3}).

3.2. Energy modelling at specific flow rates

The data reported in Tables 1, 2 and 3 were divided into training and testing data. For each flow rate 67 % data were used for model development (training) and 33 % to validate the prediction accuracy of the developed model (testing), i.e., 12 values (4 Δn in triplicate) and 6 values (2 Δn in triplicate), respectively.

Figs. 4, 5 and 6 show the prediction model of both energy recovery and specific energy at 15 $m^3\ h^{-1}$, 20 $m^3\ h^{-1}$ and 25 $m^3\ h^{-1}$ at different Δn.

A second order polynomial was applied with a very high correlation coefficient higher than 0.97 and 0.91 for E_{Rec} and e, respectively.

Figs. 7, 8, 9, 10, 11 and 12 show the models of energy recovered and specific energy at the flow rate of 15, 20 and 25 $m^3\ h^{-1}$ respectively, to which the experimental data used for testing to evaluate the correlation coefficient R^2 have been added.

The R^2 values, always higher than 0.92, demonstrate the goodness of the prediction models developed.

In Table 5 the model is further validated by the low RMSE values

Table 2
Energy consumption at $\dot{V}_s$ 15 $m^3\ h^{-1}$.

Δn [rpm]	E_{E003} [kW]		E_{E001} [kW]		E_{E002} [kW]		E_{Rec} [kW]		e [kWh m^{-3}]	
	μ	σ	μ	σ	μ	σ	μ	σ	μ	σ
3	39.99	0.19	15.12	0.10	14.11	0.07	10.77	0.35 a	1.95	0.01 a
3.2	38.84	0.20	14.85	0.16	14.06	0.06	9.94	0.40 b	1.93	0.01 ab
3.5	36.51	0.28	14.71	0.05	13.72	0.18	8.07	0.15 c	1.9	0.01 b
4	34.06	0.17	14.33	0.12	13.85	0.12	5.88	0.29 d	1.88	0.01 c
4.2	33.78	0.13	14.27	0.13	14.00	0.14	5.5	0.77 d	1.88	0.01 c
4.5	32.50	0.17	14.31	0.09	13.83	0.09	4.37	0.24 e	1.88	0.01 c

Different letters in columns denote significant statistical differences ($p < 0.05$).

Table 3
Energy consumption at $\dot{V}_s$ 20 m^3 h^{-1}.

Δn	E_{E003}		E_{E001}		E_{E002}		E_{Rec}		e	
[rpm]	[kW]		[kW]		[kW]		[kW]		[kWh m^{-3}]	
	μ	σ	μ	σ	μ	σ	μ	σ	μ	σ
3	54.49	0.38	19.78	0.11	19.06	0.05	15.65	0.40a	1.94	0.00a
3.5	47.50	0.33	19.18	0.04	18.38	0.04	9.93	0.31b	1.88	0.01b
4	45.38	0.20	18.92	0.07	18.29	0.04	8.17	0.13c	1.86	0.00b
4.5	42.11	0.21	18.56	0.11	17.96	0.05	5.58	0.05d	1.83	0.01c
5	35.56	0.26	18.04	0.06	17.21	0.10	0.31	0.32e	1.76	0.01d
6	34.92	0.07	18.00	0.05	17.34	0.05	−0.42	0.10f	1.77	0.01d

Different letters in columns denote significant statistical differences ($p < 0.05$).

Table 4
Energy consumption at $\dot{V}_s$ 25 m^3 h^{-1}.

Δn	E_{E003}		E_{E001}		E_{E002}		E_{Rec}		e	
[rpm]	[kW]		[kW]		[kW]		[kW]		[kWh m^{-3}]	
	μ	σ	μ	σ	μ	σ	μ	σ	μ	σ
4.3	52.69	0.08	20.54	0.02	19.95	0.02	12.21	0.23a	1.62	0.01b
4.4	52.35	0.10	20.49	0.02	19.77	0.01	12.09	0.29a	1.61	0.01bc
4.5	52.05	0.08	20.63	0.02	19.20	0.02	12.21	0.14a	1.6	0.01c
4.6	51.44	0.03	20.62	0.01	18.72	0.02	12.1	0.16a	1.58	0.01d
4.8	50.75	0.08	20.39	0.02	19.82	0.01	10.54	0.17b	1.61	0.00bc
4.9	50.81	0.08	20.94	0.03	20.24	0.02	9.63	0.36c	1.65	0.01a

Different letters in columns denote significant statistical differences ($p < 0.05$).

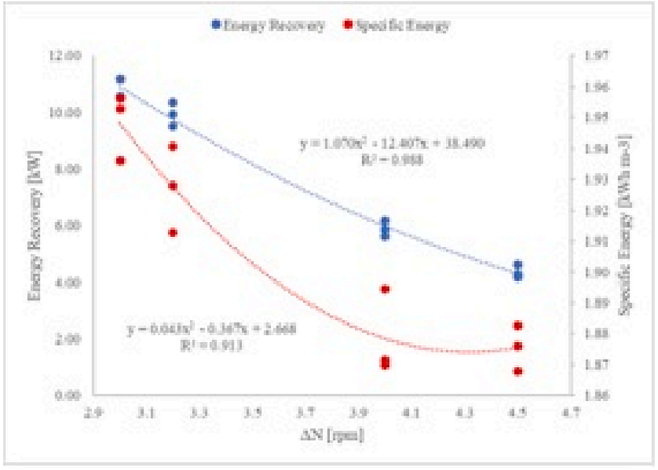

Fig. 4. Energy model for ERec and e at $\dot{V}_s$ 15 m^3 h^{-1} in its operating range of Δn.

found, confirming the reliability of the models in predicting the electrical consumption of the decanter during the sludge dewatering phase.

3.3. Energy modelling versus flow rates

The general model of the electric consumption of the decanter as a function of the flow rate was developed using the best performance data of the measurements carried out at the flow rates of 15 m^3 h^{-1}, 20 m^3 h^{-1} and 25 m^3 h^{-1}, while for the validation of the model the data of the experimental electricity consumption obtained at the flow rates of 18 m^3 h^{-1} and 22 m^3 h^{-1} (See Table 6).

In Fig. 13 the models of energy recovery and specific energy are shown.

As for the specific models exposed above, also in this case a second order polynomial correlates with R^2 above 0.99.

Figs. 14 and 15 show the models developed and integrated with the testing data. The correlation coefficient greater than 96 % and low RMSE values (Table 7) validate the high accuracy of the prediction model.

The model developed can therefore be used to predict the energy consumption of the decanter as a function of the feed flow rate.

A better discussion of the obtained results about the potential applications of the developed models will be completed at a later date.

3.4. Dryness of the waste and cake

As previously reported, the main performance result of the decanter concerns the percentage of dryness of the outgoing cake. Its potential uses will depend on this feature. The greater the dryness of the cake, the higher its quality and the greater the performance of the decanter.

In Table 8 the dry matter content of the incoming wastewater and the outgoing cake are reported for all the tests carried out at the five chosen flow rates.

The data show that in all the tests carried out there is no significant difference in the dry matter content of the incoming wastewater, this confirms the goodness of the experimental plan carried out. A difference in dry matter of the incoming wastewater for the different tests would certainly have influenced the electricity consumption, nullifying the entire experimental plan.

Furthermore, for all the flow rates analysed, as the Δn increases, the dry matter content in the cake decreases according to a second-order polynomial trend (Figs. 16–20). This result is easily explained given that increasing the Δn increases the unloading speed of the auger by decreasing the sludge residence time in the bowl, consequently its dry matter content is reduced.

Finally, as the feed rate increases, despite the adjustment of the Δn, the dry matter content in the cake is constant up to the rate of 20 m^3 h^{-1}, then it has a significant decrease at the rates of 22 m^3 h^{-1} and 25 m^3 h^{-1} as shown in Fig. 21.

3.5. Discussion and potential applications

To obtain more information from the achieved results the proposed models can be integrated with process indicators such as flow rate of the decanter and dryness of the outgoing cake.

The specific energy models explain that at 15 m^3 h^{-1} the energy

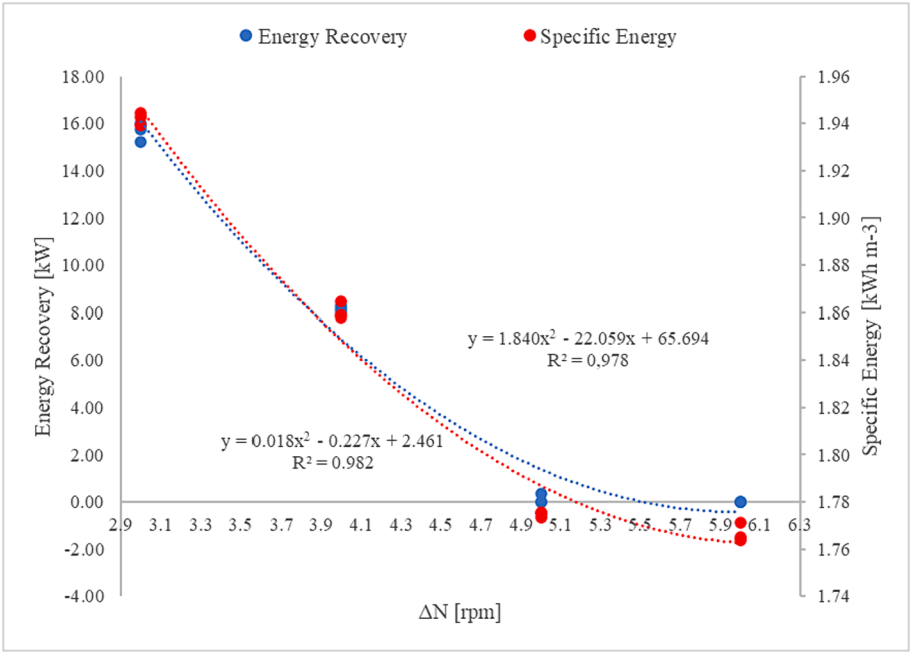

Fig. 5. Energy model for ER_{ec} and e at $\dot{V}_s$ 20 $m^3\ h^{-1}$ in its operating range of Δn.

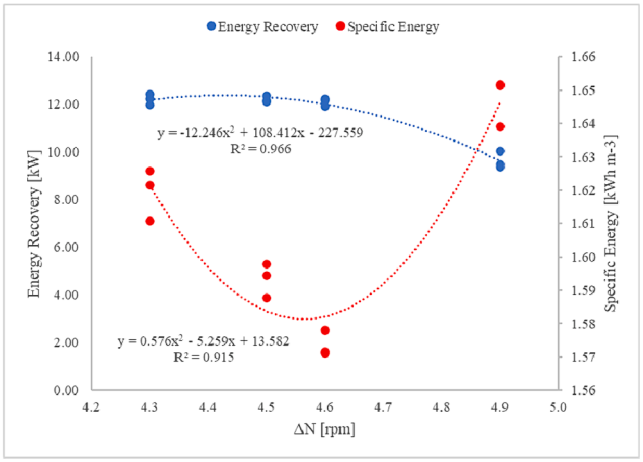

Fig. 6. Energy model for ER_{ec} and e at $\dot{V}_s$ 25 $m^3\ h^{-1}$ in its operating range of Δn.

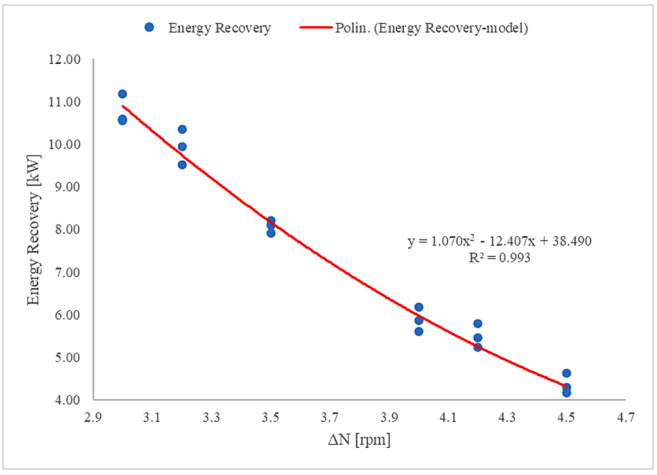

Fig. 7. Energy recovery prediction model at $\dot{V}_s$ 15 $m^3\ h^{-1}$ in its operating range of Δn.

recovery and specific energy both decrease when Δn increases in its operating range. In particular, the specific energy model has a much flatter trend with respect to the recovered energy as Δn increases. This implies that once the Δn 4.0 value has been exceeded, the absorption from the mains is almost the same and the Δn value can be set according to the desired dewatering of the sludge. Since the energy recovered above Δn 4.0 continued to decrease while the specific energy was almost constant, this means that the main motor request decreased. This is mainly due to the fact that a higher differential speed produces less dense sludges with a consequent reduction of the resistant torque. At 20 $m^3\ h^{-1}$, when the Δn reached 5.0 rpm the energy recovery is almost zero, and at 6.0 rpm the back-drive starts to request a small amount of energy. In general, the specific energy has the same behaviour of the energy recovery and above Δn 5.0 its value is almost constant. At the maximum flow rate of 25 $m^3\ h^{-1}$ the Δn operating range is very limited (since the decanter is near its upper limit) and the value of lower specific energy consumption is placed in the middle of it (Δn 4.5–4.6). In addition, the energy recovery trend from 4.3 to 4.6 rpm is almost constant and then starts to decrease. Therefore, it is advisable to operate the decanter in the first part of this range according to the desired quality of the output product. As for the general models, when processing at flow rates between 15 $m^3\ h^{-1}$ and 20 $m^3\ h^{-1}$, the energy recovered from the back-drive motor and the specific energy of the decanter both tend to decrease; on the contrary, by exceeding the flow rate of 20 $m^3\ h^{-1}$ up to 25 $m^3\ h^{-1}$ the recovered energy tends to increase while the specific energy continues to gradually decrease. This could be explained by the fact that as the flow rate increases, the operating Δn, and therefore also that for the best energy consumption, begin to decrease causing the resistant torque to increase again.

On the other hand, however, by increasing the feed rates, the dry matter content in the cake tends to decrease significantly. At the flow rate of 20 $m^3\ h^{-1}$ from the value of Δn 4.5 onwards the dry matter content is less than 20 %, the limit value below which dehydration is no longer efficient.

Therefore, by crossing the energy models with the performance results of the decanter, the specific energy and the cake dryness have

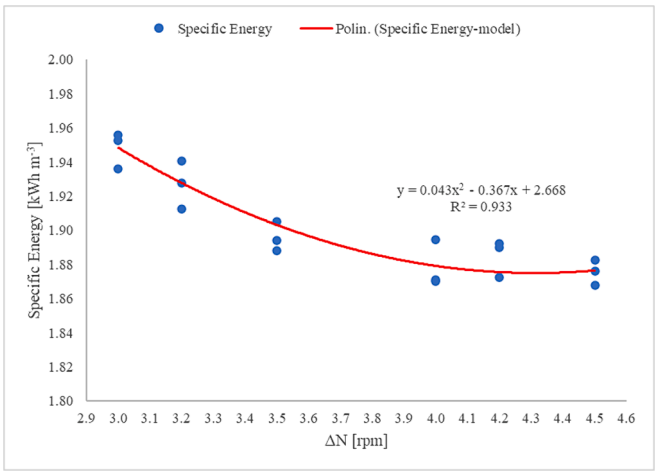

Fig. 8. Specific energy prediction model at $\dot{V}_s$ 15 m^3 h^{-1} in its operating range of Δn.

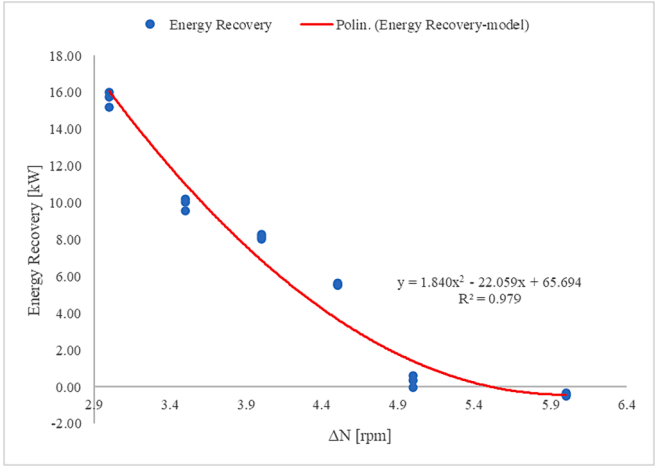

Fig. 9. Energy recovery prediction model at $\dot{V}_s$ 20 m^3 h^{-1} in its operating range of Δn.

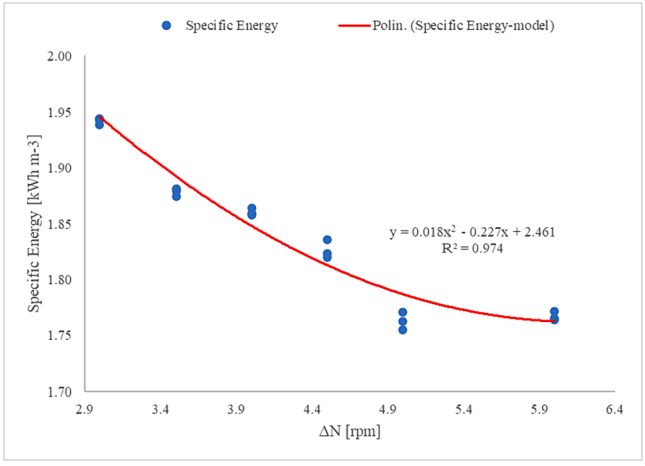

Fig. 10. Specific energy prediction model at $\dot{V}_s$ 15 m^3 h^{-1} in its operating range of Δn.

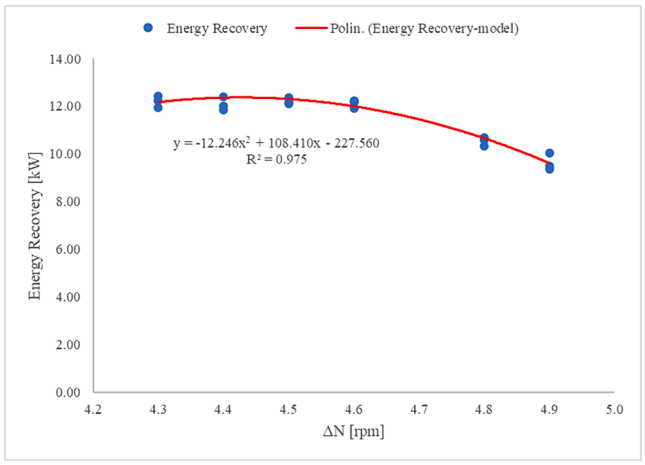

Fig. 11. Energy model for E_{Rec} and e at $\dot{V}_s$ 25 m^3 h^{-1} in its operating range of Δn.

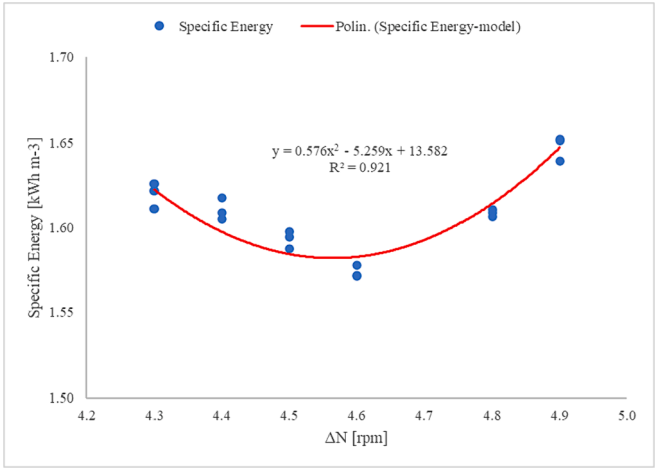

Fig. 12. Specific energy prediction model at $\dot{V}_s$ 25 m^3 h^{-1} in its operating range of Δn.

Table 5
Validation test results – RMSE for both recovery energy ERec and specific energy e.

$\dot{V}_s$ [m^3 h^{-1}]	Training values		Testing values		Whole dataset	
	$RMSE_{ERec}$	$RMSE_e$	$RMSE_{ERec}$	$RMSE_e$	$RMSE_{ERec}$	$RMSE_e$
15	2,96E-01	9,65E-03	2,63E-01	1,17E-02	2,86E-01	1,04E-02
20	8,37E-01	1,49E-02	1,56E+00	1,48E-02	1,16E+00	1,46E-02
25	2,09E-01	8,25E-03	2,88E-01	1,07E-02	2,38E-01	9,15E-03

opposite trends and the models developed demonstrate this.

Based on the surveyed data the developed models can be utilized by the process planners to predict energy consumption depending on the decanter adjustment parameters and to identify the most energy-efficient process which also meets the best dryness result of the cake coming out of the decanter.

4. Conclusion

Energy consumption leads to an increase in the carbon footprint with

Table 6
Shows the data of the measurements at 18 $m^3\ h^{-1}$ and 22 $m^3\ h^{-1}$.

$\dot{V}_s$ $m^3\ h^{-1}$	Δn [rpm]	E_{E003} [kW]		E_{E001} [kW]		E_{E002} [kW]		E_{Rec} [kW]		e [kWh m^{-3}]	
		μ	σ	μ	Σ	μ	σ	μ	σ	μ	σ
18	3	47.57	0.99	17.36	0.07	16.57	0.08	13.64	0.98	1.88	0.98
18	4	39.05	0.06	16.58	0.06	15.97	0.05	6.50	0.00	1.81	0.00
18	5	34.46	0.25	16.19	0.10	15.94	0.10	2.33	0.35	1.79	0.35
22	4	40.96	0.39	16.71	0.17	16.41	0.12	7.84	0.26	1.51	0.26
22	5	38.44	0.35	16.79	0.12	16.16	0.06	5.49	0.19	1.50	0.19
22	6	45.16	0.39	19.97	0.06	19.13	0.16	6.06	0.19	1.78	0.19

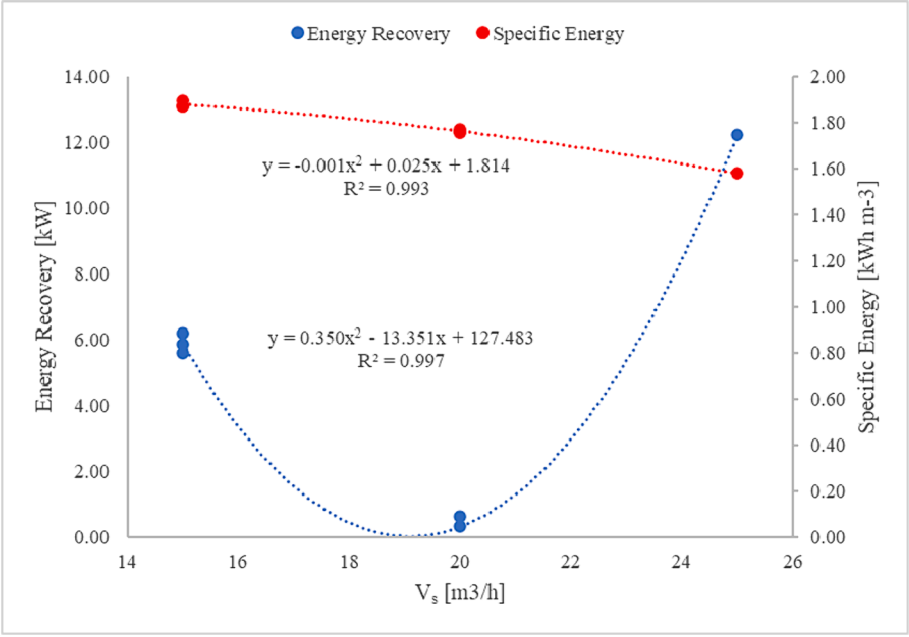

Fig. 13. Energy model for E_{Rec} and e versus flow rate.

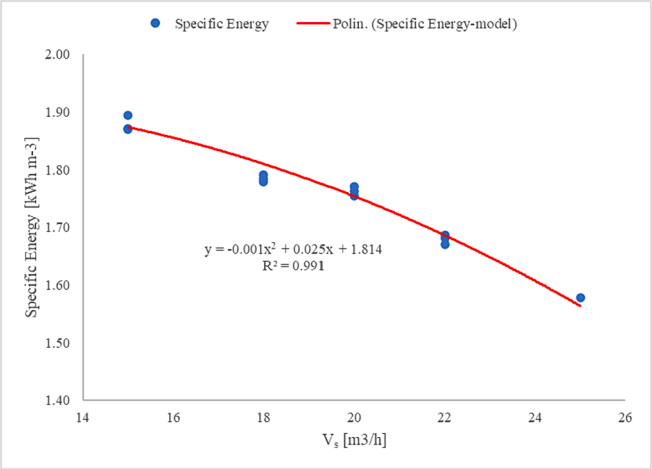

Fig. 14. Energy recovery prediction versus flow rate.

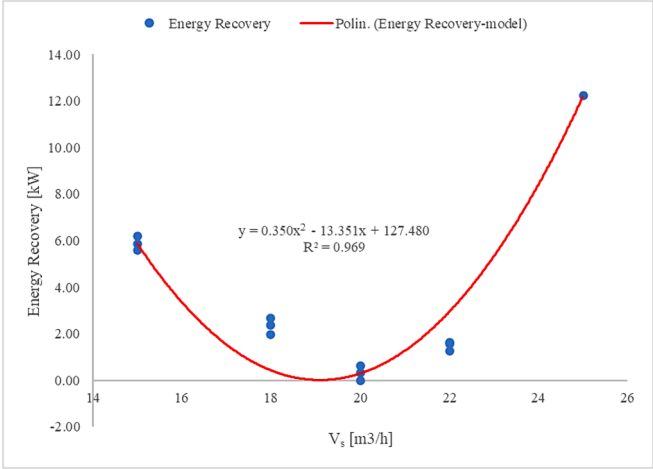

Fig. 15. Specific energy prediction model versus flow rate.

a high risk linked to climate change. Statistics also predict that in the coming years, also as a result of a constant demographic increase, energy consumption will continue to increase.

Implementing energy saving strategies not only on a large scale but also on a medium and small scale is the basis for the rationalization of energy consumption. The energy modelling of the consumption of machines driven by electric motors is recognized by the scientific community as a valid method for the accurate prediction of consumption; however, in order for the models to be reliable it is necessary to adapt them to the individual machines for the different conditions of use.

In this scientific work, we created the energy modelling of a decanter

Table 7
Validation of general model – RMSE for both recovery energy ERec and specific energy e.

	RMSE [kW]	R^2 [-]
E_{Rec}	1,90E-00	96,88
e	2,59E-02	99,06

already implemented with an energy saving system (VFD with regenerative braking), during the dewatering of urban and industrial sludge.

The energy models at 15–20–25 $m^3\ h^{-1}$ were used to obtain the optimal operational conditions in the specific ranges of differential speed Δn between the bowl and screw of the decanter centrifuge. Starting from specific models, general models in terms of energy efficiency were derived. The main results obtained with general prediction models highlight that the specific energy decreases with the increase of sludge flow rate, passing from 1.88 kWh m^{-3} to 1.57 kWh m^{-3} when the flow rate changes from 15 to 25 $m^3\ h^{-1}$. As for the energy recovery, it

Table 8
Dry matter content of wastewater and cake.

Sludge flow rate [$m^3\ h^{-1}$]	Δ n [rpm]	Total Incoming waste (dm) [%]			Outgoing cake (dm) [%]		Total Outgoing cake (dm) [%]		
		μ	σ		μ	σ	μ	σ	
15	3	1.77 %	0.24 %	a	22.36 %	0.05 %	20.46 %	1.12 %	a
15	3.2				20.94 %	0.18 %			
15	3.5				20.36 %	0.24 %			
15	4				20.25 %	0.29 %			
15	4.2				19.93 %	0.07 %			
15	4.5				18.77 %	0.17 %			
18	3	1.87 %	0.25 %	a	20.63 %	0.18 %	20.47 %	0.21 %	ab
18	4				20.46 %	0.23 %			
18	5				20.33 %	0.15 %			
20	3	1.72 %	0.18 %	a	20.63 %	0.51 %	19.46 %	1.35 %	ab
20	3.5				20.43 %	0.14 %			
20	4				20.22 %	0.06 %			
20	4.5				19.63 %	0.22 %			
20	5				18.99 %	0.66 %			
20	6				16.89 %	0.30 %			
22	4	1.74 %	0.43 %	a	19.99 %	0.24 %	19.45 %	0.47 %	b
22	5				19.23 %	0.02 %			
22	6				19.13 %	0.39 %			
25	4.3	1.88 %	0.26 %	a	19.43 %	0.16 %	19.21 %	0.17 %	b
25	4.4				19.32 %	0.10 %			
25	4.5				19.21 %	0.07 %			
25	4.6				19.16 %	0.05 %			
25	4.8				19.14 %	0.14 %			
25	4.9				19.02 %	0.17 %			

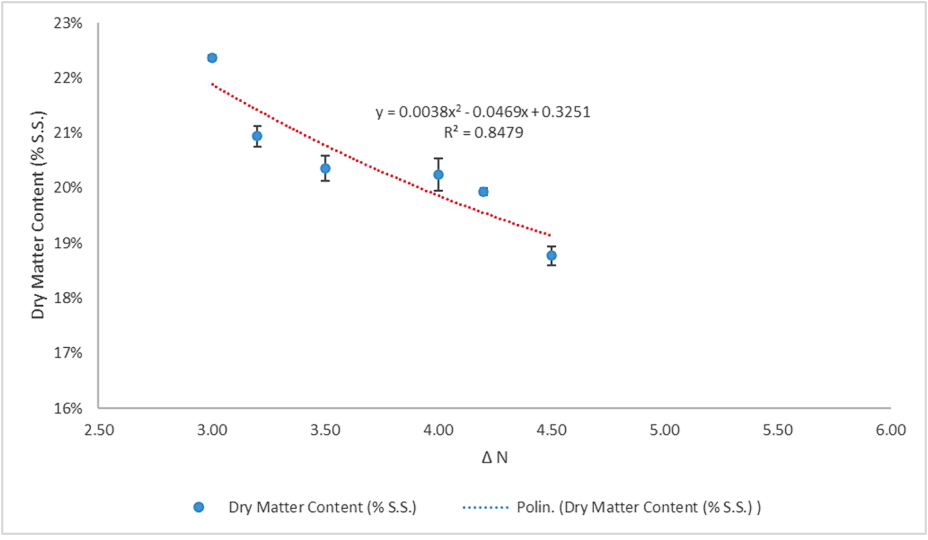

Fig. 16. Dry matter content in the cake versus Δn,$\dot{V}_s$ 15 $m^3\ h^{-1}$.

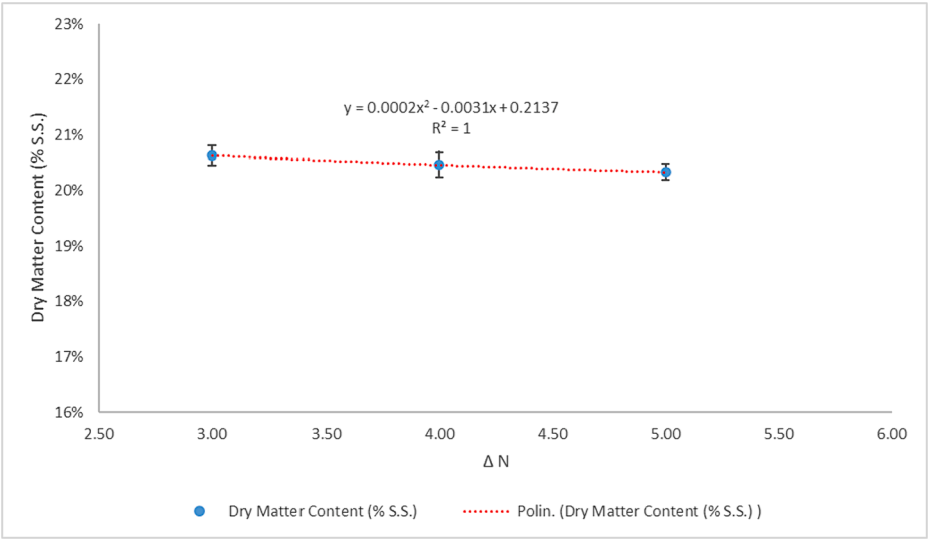

Fig. 17. Dry matter content in the cake versus Δn, $\dot{V}_s$ 18 m^3 h^{-1}.

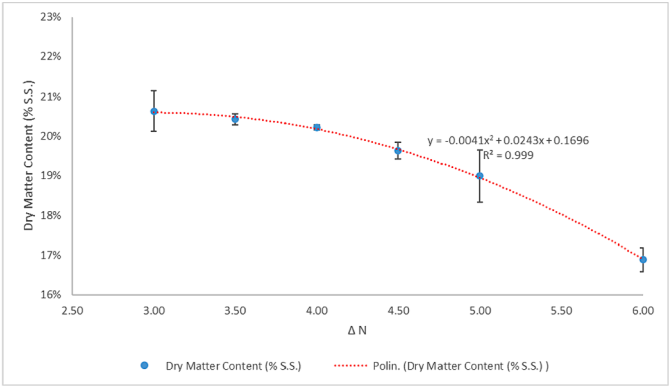

Fig. 18. Dry matter content in the cake versus Δn, $\dot{V}_s$ 20 m^3 h^{-1}.

decreased until a flow rate of 20 m^3 h^{-1}, after that it started increasing again due to a decrease of operative Δn, which implies an increase of the resistant torque. The dry matter content in the cake decreases when the Δn increases or when the feed rate increases.

The accuracy of the models was confirmed with correlation coefficients R^2 always above 0.92 and very low values of Root Mean Square Error (RMSE).

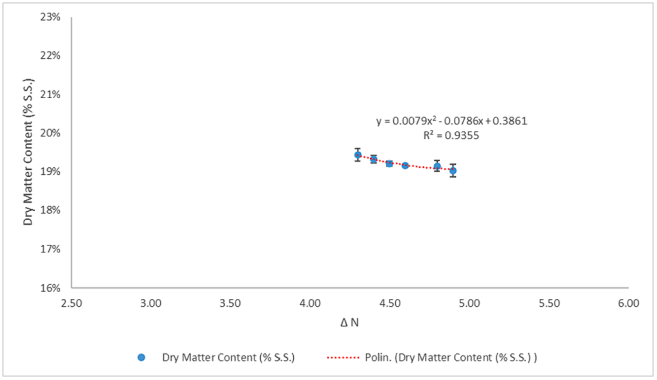

Fig. 20. Dry matter content in the cake versus Δn, $\dot{V}_s$ 25 m^3 h^{-1}.

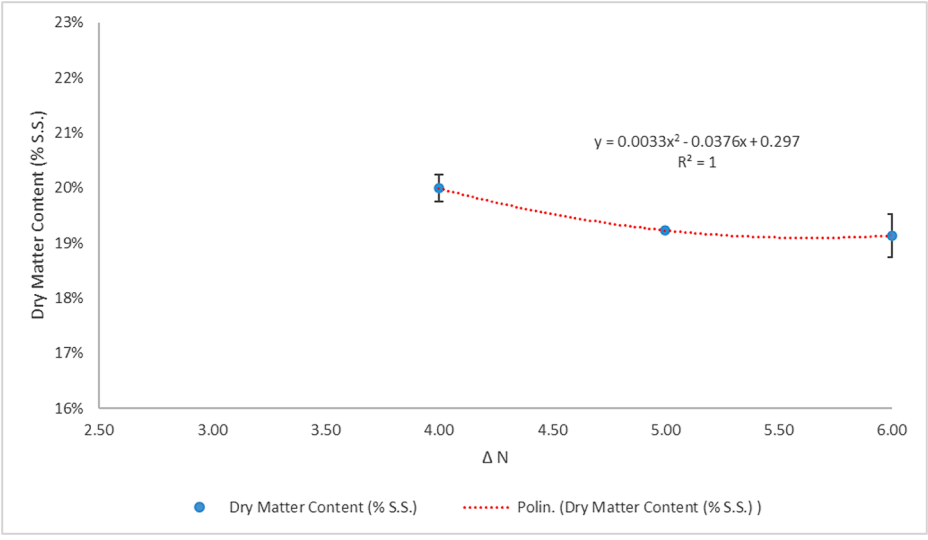

Fig. 19. Dry matter content in the cake versus Δn, $\dot{V}_s$ 22 m^3 h^{-1}.

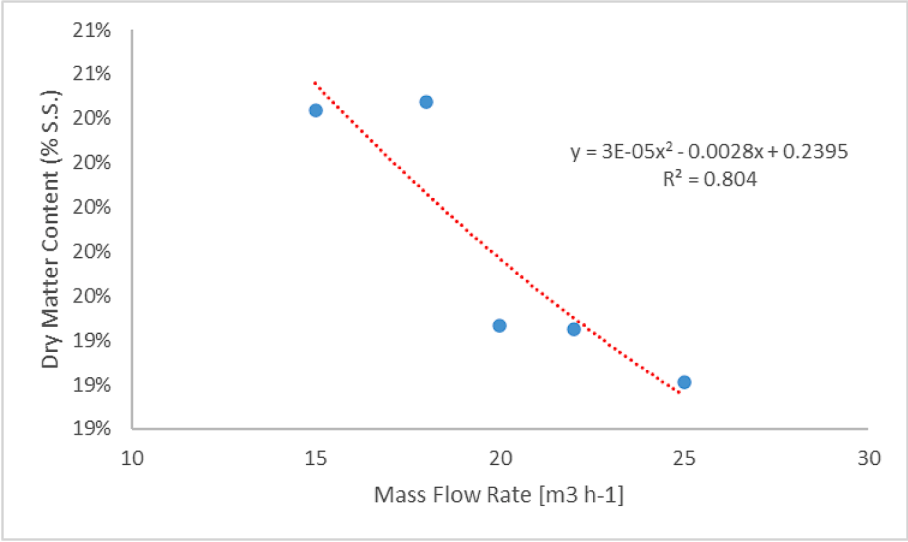

Fig. 21. Dry matter content in the cake versus flow rate.

The developed models, placed in the hands of the process planner, could provide useful information to be able to set up the sludge dewatering process with the aim, on the one hand of reaching the chosen level of dryness of the outgoing sludge (currently the only objective), and on the other hand of identifying the correct adjustment of the decanter which leads, at the same time, to the maximum level of energy savings.

Availability and usage-reliable energy models will add a further step to the rationalization of energy consumption and an improvement in environmental sustainability.

CRediT authorship contribution statement

Alessandro Leone: Writing – review & editing, Validation. **Claudio Perone:** Supervision, Data curation. **Antonio Berardi:** Writing – original draft, Methodology. **Antonia Tamborrino:** Writing – original draft, Validation.

Declaration of competing interest

The authors declare that they have no known competing financial interests or personal relationships that could have appeared to influence the work reported in this paper.

Data availability

No data was used for the research described in the article.

References

[1] Majewski S, Mentel U, Salahodjaev R, Cierpiał-Wolan M. Electricity consumption and economic growth: evidence from South Asian countries. Energies 2022;15:1327. https://doi.org/10.3390/en15041327.
[2] Navarro CEB, Álvarez-Quiroz VJ, Sampi J, Sánchez AAA. Does economic growth promote electric power consumption? Implications for electricity conservation, expansive, and security policies. Electricity J 2023;36(1):107235. https://doi.org/10.1016/j.tej.2023.107235. ISSN 1040-6190.
[3] Shafiei S, Salim RA. Non-renewable and renewable energy consumption and CO2 emissions in OECD countries: A comparative analysis. Energy Policy 2014;66:547–56. https://doi.org/10.1016/j.enpol.2013.10.064. ISSN 0301-4215.
[4] Achuo ED, Miamo CW, Nchofoung TN. Energy consumption and environmental sustainability: What lessons for posterity? Energy Reports 2022;8:12491–502. https://doi.org/10.1016/j.egyr.2022.09.033. ISSN 2352-4847.
[5] Kocak E, Ulug EE, Oralhan B. The impact of electricity from renewable and non-renewable sources on energy poverty and greenhouse gas emissions (GHGs): Empirical evidence and policy implications. Energy 2023;272:127125. https://doi.org/10.1016/j.energy.2023.127125. ISSN 0360-5442.
[6] Khanlari A, Sozen A, Sirin C, Tuncer AD, Gungor A, Gungor A. Performance enhancement of a greenhouse dryer: analysis of a cost-effective alternative solar air heater. J Clean Prod 2020;251. https://doi.org/10.1016/j.jclepro.2019.119672.
[7] Zhao J, Dong K, Dong X, Shahbaz M. How renewable energy alleviate energy poverty? A global analysis. Renewable Energy 2022;186:299–311. https://doi.org/10.1016/j.renene.2022.01.005. ISSN 0960-1481.
[8] Xin D, Ahmad M, Khattak SI. Impact of innovation in climate change mitigation technologies related to chemical industry on carbon dioxide emissions in the United States. J Clean Prod 2022;379(Part 1):134746. https://doi.org/10.1016/j.jclepro.2022.134746. ISSN 0959-6526.
[9] Yasin I, Ahmad N, Chaudhary MA. Catechizing the environmental-impression of urbanization, financial development, and political institutions: a circumstance of ecological footprints in 110 developed and less-developed countries. Soc Indic Res 2020;(2).
[10] Xu B, Wang T, Ma D, Song R, Zhang M, Gao L, et al. Impacts of regional emission reduction and global climate change on air quality and temperature to attain carbon neutrality in China. Atmos Res 2022;279:106384. https://doi.org/10.1016/j.atmosres.2022.106384. ISSN 0169-8095.
[11] Korkmaz ME, Günay M. Finite element modelling of cutting forces and power consumption in turning of AISI 420 martensitic stainless steel. Arabian J Sci Eng 2018;43:4863–70. https://doi.org/10.1007/s13369-018-3204-4.
[12] Pimenov DY, Mia M, Gupta MK, Machado AR, Pintaude G, Unune DR, et al. Resource saving by optimization and machining environments for sustainable manufacturing: A review and future prospects. Renew Sustain Energy Rev 2022;166:112660. https://doi.org/10.1016/j.rser.2022.112660. ISSN 1364-0321.
[13] Handzel J. Extending pump life while saving energy requires proper motor sizing. *World Pumps* 2022;2002(431):38. https://doi.org/10.1016/S0262-1762(02)80204-8. ISSN 0262-1762.
[14] Wei C, Li Y, Li L, Lai K, Jia S, Xie J, et al. Energy saving and high efficiency production oriented forward-and-reverse multidirectional turning: Energy modeling and application. Energy 2022;252:123981. https://doi.org/10.1016/j.energy.2022.123981. ISSN 0360-5442.
[15] Zhou B, Qi Y, Liu Y. Proactive preventive maintenance policy for buffered serial production systems based on energy saving opportunistic windows. J Clean Prod 2020;253:119791. ISSN 0959-6526.
[16] Bai C, Park H, Wang L. A model-based parametric study of centrifugal dewatering of mineral slurries. Minerals 2022;12:1288. https://doi.org/10.3390/min12101288.
[17] Gómez JR, Sousa V, Eras JJC, Gutiérrez AS, Viego PR, Quispe EC, et al. Assessment criteria of the feasibility of replacement standard efficiency electric motors with high-efficiency motors. Energy 2022;239(Part A):121877. https://doi.org/10.1016/j.energy.2021.121877. ISSN 0360-5442.
[18] Tan C, Feng Z, Liu X, Fan J, Cui W, Sun R, et al. Review of variable speed drive technology in beam pumping units for energy-saving. Energy Rep 2020;6:2676–88. https://doi.org/10.1016/j.egyr.2020.09.018. ISSN 2352-4847.
[19] Wang Y, He Y, Li Y, Yan P, Feng L. An analysis framework for characterization of electrical power data in machining. Int J Precis Eng Manuf 2015;16:2717–23. https://doi.org/10.1007/s12541-015-0347-z.
[20] Lv J, Tang R, Tang W, Jia S, Liu Y, Cao Y. An investigation into methods for predicting material removal energy consumption in turning. J Clean Prod 2018;193:128–39. https://doi.org/10.1016/j.jclepro.2018.05.035.
[21] Pawanr S, Garg GK, Routroy S. A novel approach to model the energy consumption of machine tools for machining cylindrical parts. J Manuf Process 2022;84:28–42. https://doi.org/10.1016/j.jmapro.2022.09.040. ISSN 1526-6125.
[22] Egware HO, Obanor AI. The investigation of an SGT5-2000E gas turbine power plant performance in Benin City based on energy analysis. Energy Convers Manage:

X 2022;16:100316. https://doi.org/10.1016/j.ecmx.2022.100316. ISSN 2590-1745.
[23] Armarego EJA, Ostafiev D, Wong SWY, Verezub S. An appraisal of empirical modeling and proprietary software databases for performance prediction of machining operations. Mach Sci Technol 2000;4(3):479–510.
[24] Balogun VA, Mativenga PT. Modelling of direct energy requirements in mechanical machining processes. J Clean Prod 2013;41:179–86.
[25] Garg A, Lam JSL, Gao L. Power consumption and tool life models for the production process. J Clean Prod 2016;131:754–64.
[26] Tamborrino A, Catalano F, Berardi A, Bianchi B. New modelling approach for the energy and steam consumption evaluation in a fresh pasta industry. Chem Eng Trans 2021;87:409–14.
[27] Perone C, Berardi A, Dellisanti CD, Tamborrino A, Leone A. Investigation of an energy-saving system to reduce the energy consumption of decanter machine. Chem Eng Trans 2023;102:2023. https://doi.org/10.3303/CET23102027.
[28] Tamborrino A, Perone C, Catalano F, Squeo G, Caponio F, Bianchi B. Modelling energy consumption and energy-saving in high-quality olive oil decanter centrifuge: Numerical study and experimental validation. Energies 2019;12(13):2592.
[29] Catalano F, Perone C, Iannacci V, Leone A, Tamborrino A, Bianchi B. Energetic analysis and optimal design of a CHP plant in a frozen food processing factory through a dynamical simulation model. Energy Convers Manage 2020;225:113444. https://doi.org/10.1016/j.enconman.2020.113444. ISSN 0196-8904.
[30] Perone C, Romaniello R, Leone A, Berardi A, Tamborrino A. Towards energy efficient scheduling in the olive oil extraction industry: Comparative assessment of energy consumption in two management models, *Energy Conversion and Management: X*, Volume 16. ISSN 2022;100287:2590. https://doi.org/10.1016/j.ecmx.2022.100287.
[31] Tamborrino A, Mescia L, Taticchi A, Berardi A, Lamacchia C, Leone A, et al. Continuous pulsed electric field pilot plant for olive oil extraction process. Innov Food Sci Emerg Technol 2022;82:103192. https://doi.org/10.1016/j.ifset.2022.103192. ISSN 1466-8564.
[32] Tamborrino A, Berardi A, de Lillo E, Ragone G, De Benedictis M, Tufariello M, et al. Using a continuous microwave system for postharvest almond disinfestation. Postharvest Biol Technol 2023;201:112369. ISSN 0925-5214.
[33] Aykut Ş, Gölcü M, Semiz S, Ergür HS. Modeling of cutting forces as function of cutting parameters for face milling of satellite 6 using an artificial neural network. J Mater Process Technol 2007;190(1–3):199–203.
[34] Chu CP, Lee DJ. Dewatering of waste activated sludge via centrifugal field. Drying Technol 2002;20(4–5):953–66.
[35] Laval A. Decanter centrifuge technology-Separating solids from liquids. PPM00025EN 2016;304:1–7.
[36] Tamborrino A, Leone A, Romaniello R, Catalano P, Bianchi B. Comparative experiments to assess the performance of an innovative horizontal centrifuge working in a continuous olive oil plant. Biosyst Eng 2015;129:160–8. https://doi.org/10.1016/j.biosystemseng.2014.10.005. ISSN 1537-5110.
[37] Beveridge T, Harrison JE. Juice extraction with the decanter centrifuge: sweet and sour cherries, peaches and apricots. Food Res Int 1995;28(2):173–7. https://doi.org/10.1016/0963-9969(95)90802-H. ISSN 0963-9969.
[38] Beveridge T, Harrison JE, Gayton RR. Decanter centrifugation of apple mash: effect of centrifuge parameters, apple variety and apple storage. Food Res Int 1992;25(2):125–30.
[39] Abioye KJ, Harun NY, Sufian S, Yusuf M, Kamyab H, Hassan MA, et al. Regulation of ash slagging behavior of palm oil decanter cake by alum sludge addition. *Chemosphere* 2023:138452. https://doi.org/10.1016/j.chemosphere.2023.138452. ISSN 0045-6535.
[40] Schubert T, Meric A, Boom R, Hinrichs J, Atamer Z. Application of a decanter centrifuge for casein fractionation on pilot scale: Effect of operational parameters on total solid, purity and yield in solid discharge. Int Dairy J 2018;84:6–14. https://doi.org/10.1016/j.idairyj.2018.04.002. ISSN 0958-6946.
[41] Ginisty P, Mailler R, Rocher V. Sludge conditioning, thickening and dewatering optimization in a screw centrifuge decanter: Which means for which result? J Environ Manage 2021;280:111745.
[42] Qasim SR, Zhu G. Wastewater Treatment and Reuse Theory and Design Examples, Volume 2: Post-Treatment, Reuse, and Disposal. CRC Press; 2017.
[43] Bell GRA, Symons DD, Pearse JR. Mathematical model for solids transport power in a decanter centrifuge. Chem Eng Sci 2014;107:114–22. https://doi.org/10.1016/j.ces.2013.12.007. ISSN 0009-2509,.
[44] Leone A, Romaniello R, Zagaria R, Tamborrino A. Mathematical modelling of the performance parameters of a new decanter centrifuge generation. J Food Eng 2015;166:10–20. https://doi.org/10.1016/j.jfoodeng.2015.05.011. ISSN 0260-8774.
[45] Catalano P, Pipitone F, Calafatello A, Leone A. Productive efficiency of decanters with short and variable dynamic pressure cones. Biosyst Eng 2003;86(4):459–64. https://doi.org/10.1016/j.biosystemseng.2003.08.011. ISSN 1537-5110.
[46] Squeo G, Tamborrino A, Pasqualone A, Leone A, Paradiso VM, Summo C, et al. Assessment of the influence of the decanter set-up during continuous processing of olives at different pigmentation index. Food Bioprocess Technol 2017;10:592–602. https://doi.org/10.1007/s11947-016-1842-7.
[47] Raghava M, Naik MGC. Comparative study of recent advancements in regenerative drives in elevator systems. Int J Electr Electr Eng Telecoms 2014;3:56–68.
[48] Ram S, Rahi OP, Sharma V. A comprehensive literature review on slip power recovery drives. Renew Sustain Energy Rev 2017;73:1364. https://doi.org/10.1016/j.rser.2016.11.154. ISSN 922-934.
[49] Rasin KR, Arunkumar G. Regeneration in variable frequency drives and energy saving methods. Int Res J Eng Technol (IRJET) 2017;4(3):1246–9. e-ISSN: 2395-0056, p-ISSN: 2395-0072.
[50] Cooperstein JL. U.S. Patent No. 5,203,762. Philadelphia, Pa: U.S. Patent and Trademark Office; 1993.
[51] Bretzius J. U.S. Patent No. 6,600,278. Washington, DC: U.S. Patent and Trademark Office; 2003.